Journal of Mathematical Modeling
Vol. -, No. -, 2026, pp. -. Research Article

JMM

Analyzing peak and late phase sensitivities in a delayed alcoholism model with Taylor wavelets

Neslişah İmamoğlu Karabaş[†], Sevin Gümgüm[‡*]

[†,‡]*Department of Mathematics, İzmir University of Economics, İzmir, Turkey*

Email(s): sevin.gumgum@ieu.edu.tr, neslisah.karabas@ieu.edu.tr

Abstract. We apply the Taylor wavelet collocation method to a nonlinear delayed Susceptible-–Drinker—Treatment—Recovered (SDTR) alcoholism model and conduct a systematic sensitivity analysis that reveals both qualitatively and quantitatively different parameter roles at the epidemic peak and at the late phase of the simulation. A fine sweep of the delay parameter τ uncovers a non-monotonic response in every compartment, with an interior extremum that has not been previously reported for this model class. Applying the method, continuous piecewise-polynomial approximations of the model were obtained without linearization. Accuracy of the method was confirmed through residual error calculations and a comparison with the MATLAB `dde23` solver on the full simulation interval. The method delivers continuous polynomial approximations on each subinterval and reproduces benchmark delay differential equations (DDE) solutions on the full simulation horizon. Sensitivity analysis was performed at both epidemic peaks and at the late phase of the simulation. It was found that parameters show significantly different behaviors over these time scales. Social transmission has marked impacts on peak burden but reverses sign at the late phase. Treatment parameters show their largest sensitivities at the late phase, with treatment-entry rate also acting strongly at the peak. Time delay produces a non-monotonic effect—each compartment exhibits an interior extremum on the plausible range $\tau \in [0,8]$, with D_{peak} maximized near $\tau \approx 2$–3 and $D(t=30)$ minimized near $\tau \approx 4$. These differences imply that controlling peaks requires different intervention strategies than controlling late-phase addiction levels.

Keywords: Alcoholism model, time delay, parametric investigation, Taylor wavelet method.
AMS Subject Classification 2020: 92D30, 65T60, 65L05, 34K06.

1 Introduction

The harmful use of alcohol is a major public health problem that contributes to approximately 3 million deaths annually and represents more than 5% of the global burden of disease [25]. Excess alcohol

*Corresponding author
Received: 10 February 2025/ Revised: 19 May 2026/ Accepted: 20 May 2026
DOI: 10.22124/jmm.2026.32955.2999

consumption harms personal health and contributes to violence, crime, and antisocial behavior [12, 14, 26]. Since alcoholism can be considered a socially contagious disease, mathematical modeling is an important tool to understand its transmission dynamics and to evaluate the effectiveness of potential control strategies [4,12,15]. Compartmental frameworks of this kind are widely used across the epidemic modeling literature; Nkeki and Mbarie [16], for example, analyzed an SEIWRV chickenpox model with weakened-immune individuals and established stability of both the disease-free and endemic equilibria.

Time delays are a natural feature of epidemic models, since infection, recovery, and treatment processes do not act instantaneously. Compartmental models incorporating delays together with saturated incidence and treatment terms have been widely analyzed in the literature [17]. In the real world, the progression of addiction is not instantaneous; there are inherent lags in behavioral change, response to treatment, and the development of dependency. There are several studies on delayed alcohol models in the literature. Huo et al. [12] developed a binge drinking model in which the time delay represents the temporary period of immunity to relapse that a person experiences after recovery. Similarly, Ma et al. [15] presented a model using a time delay to represent the latency period during which a susceptible individual becomes a heavy drinker, demonstrating how this delay can cause the instability of the system. The use of delay in the model has also been applied to incorporate distributed delays, which are regarded as more realistic because they consider that the time lag is not uniform across the population. Distributed delays are considered in the study of Wang et al. [24] and Djillali et al. [5], and an improved understanding of the dynamics of alcoholism under more heterogeneous conditions is presented. Beyond alcoholism, the role of a single delay parameter in reshaping system dynamics has also been examined in other contexts; Hadadi et al. [11] analyzed the dynamics and bifurcations of a discrete-time neural network model with a single delay. In addition, many of these advanced models are coupled with optimal control theory to identify the most effective public health interventions. Studies by Bouajaji et al. [4], Thamchai [22], and Zhang et al. [27] have all formulated delayed systems with control functions representing awareness campaigns or treatment programs.

These studies focus on stability and bifurcation analysis to identify critical thresholds. A complementary direction, less developed for delayed alcoholism models, is a quantitative parameter-by-parameter sensitivity analysis that compares peak and late-phase dynamics within the same model. Our aim is to contribute to this direction by conducting such an analysis using normalized sensitivity coefficients and discussing the qualitative implications for intervention strategies. To do that, we solve the governing system of equations using the Taylor wavelet method. Linearization of nonlinear terms is not required in this technique, which is an advantage over other numerical methods. Wavelet methods have gained attention in modeling biological systems and epidemic dynamics because they show high accuracy in approximating both long-term trends and transient states. Recent studies applied these techniques to various infectious disease models such as HIV/AIDS and Covid-19 [3, 19, 21]. Their applications have been extended to solve delay and nonlinear differential equations [6–8, 18, 20]. Spectral and polynomial collocation methods have also been applied directly to alcoholism models for parametric sensitivity analyses. Closely related polynomial collocation strategies have been used for other epidemic models with vaccination and treatment; Babayar-Razlighi [2], for instance, solved a six-compartment influenza model via a Newton–Chebyshev polynomial method on partitioned intervals. Gümgüm and Pişkin [9] investigated alcohol-induced liver disease using Chebyshev and Legendre polynomials and showed that the recovery rate of heavy drinkers is the most influential parameter for reducing disease burden. Türe and Gümgüm [23] modeled the impact of public and private treatment on alcohol addiction using Chebyshev and Laguerre spectral methods, demonstrating that treatment accessibility and recovery efficacy are the

dominant factors in long-term addiction control. Gümgüm [10] extended this line of research to diabetic populations, applying the Gegenbauer wavelet method to a six-compartment model and showing that social interaction parameters and treatment access carry the highest sensitivity coefficients.

The present paper makes three contributions relative to the existing literature on delayed alcoholism models. First, we provide a complete Taylor-wavelet collocation treatment of the Bouajaji et al. [4] model, including an explicit history function, a corrected and fully specified algebraic system, and an operational matrix whose general entry formula is derived in closed form; these details are absent from the source paper and from prior wavelet studies on epidemic DDEs. Second, we conduct a systematic normalized sensitivity analysis at two characteristic times—the epidemic peak and the late phase—using two-sided finite-range secant approximations on biologically plausible parameter ranges. The comparison reveals that social transmission and inhibition parameters govern peak burden but have minimal late-phase effect, whereas treatment and recovery parameters dominate the late phase; this temporal classification has not been reported for this model. Third, a fine τ-sweep over the plausible range $\tau \in [0,8]$ reveals that the delay parameter produces a *non-monotonic* response in every compartment: each compartment has an interior extremum, with D_{peak} maximized near $\tau \approx 2$–3 and $D(t=30)$ minimized near $\tau \approx 4$. To our knowledge this non-monotonic delay effect has not been identified in prior analytical or numerical studies of this model class. We do not claim methodological novelty for the Taylor wavelet scheme itself, which has been applied to related biological systems in [3,8,19,20]; the contribution is the application to a delayed SDTR system together with the parametric findings that the application enables.

The paper is organized as follows. Section 2 presents the formulation of the delayed mathematical model. Section 3 details the methodology of the Taylor wavelet method and its application to the system. In Section 4, we present the numerical validation through residual error analysis and comparison with benchmark solvers. Section 5 contains the numerical simulations and parametric sensitivity analysis. Finally, Section 6 discusses the implications of our findings and summarizes our conclusions.

2 Delayed mathematical model

In this study, we consider a mathematical model to explore the impact of the model parameters on the dynamics of alcohol consumption based on the framework of a delayed SDTR system given in [4].

2.1 Model assumptions and structure

The SDTR model shows that the transition to heavy drinking is not instantaneous. Moderate or occasional drinkers, when influenced by heavy drinkers, experience a latency period before presenting similar behaviors. A discrete time delay, represented by τ, is proposed to describe this. Moreover, the model implements a modified saturated incidence rate. This mechanism avoids the unlimited growth of new heavy drinkers. With a rising number of moderate drinkers, the rate at which new heavy drinkers enter saturates because of factors including awareness or limited opportunities for interaction. The population of moderate drinkers is modeled according to a logistic growth pattern, representing natural limits on population size. The population is divided into four different subpopulations:

- $S(t)$: Moderate and occasional drinkers, who are susceptible to becoming heavy drinkers.
- $D(t)$: Heavy drinkers (addicted).

- $T(t)$: Drinkers currently in treatment.
- $R(t)$: Drinkers who are temporarily recovered but may relapse.

The transitions between these compartments are represented in Figure 1.

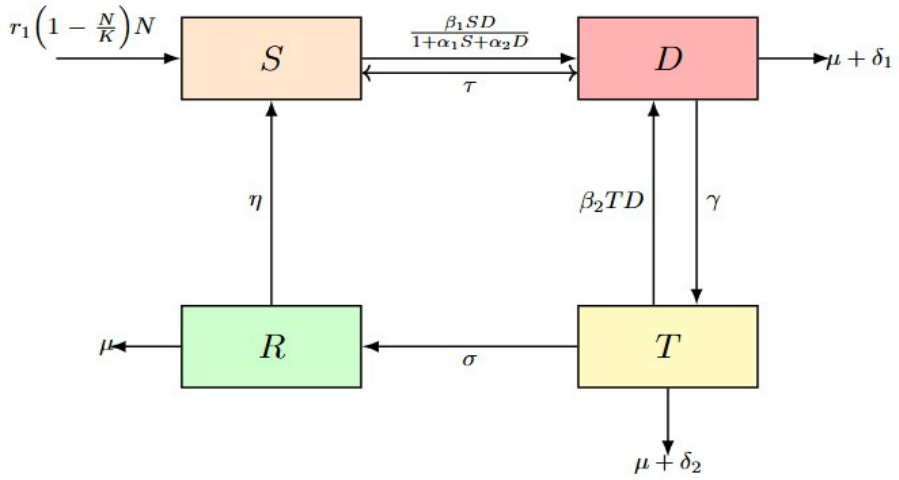

Figure 1: Flowchart of the delayed alcoholism model. The transition from the susceptible compartment S to the heavy-drinker compartment D incorporates a discrete time delay τ representing the latency period; the effective rate of this transition is multiplied by the survival factor $e^{-\mu\tau}$ to account for natural mortality during the latency period.

2.2 The system of delay differential equations

The dynamics of the system is governed by the following set of delay differential equations [4]:

$$\begin{aligned}
\frac{dS}{dt} &= r_1\left(1-\frac{N(t)}{K}\right)N(t) - \frac{\beta_1 S(t)D(t)}{1+\alpha_1 S(t)+\alpha_2 D(t)} + \eta R(t),\\
\frac{dD}{dt} &= e^{-\mu\tau}\frac{\beta_1 S(t-\tau)D(t-\tau)}{1+\alpha_1 S(t-\tau)+\alpha_2 D(t-\tau)} + \beta_2 T(t)D(t) - (\mu+\delta_1+\gamma)D(t),\\
\frac{dT}{dt} &= \gamma D(t) - \beta_2 T(t)D(t) - (\mu+\delta_2+\sigma)T(t),\\
\frac{dR}{dt} &= \sigma T(t) - (\mu+\eta)R(t),
\end{aligned} \tag{1}$$

where $N(t) = S(t)+D(t)+T(t)+R(t)$ represents the total population at time t. The term $e^{-\mu\tau}$ accounts for the natural mortality of individuals during the incubation period τ.

The initial conditions for the compartmental populations are carefully chosen to reflect realistic scenarios encountered in communities with moderate to high alcohol consumption patterns. The susceptible population begins at $S(0) = 200$ individuals, representing those at risk of developing alcohol dependency.

The population with alcohol dependency starts at $D(0) = 70$ individuals, while the population undergoing treatment is initialized at $T(0) = 20$ individuals. The recovered population begins at $R(0) = 20$ individuals, and consequently, the total population at the initial time is $N(0) = 310$ individuals. These initial values are established based on population-level data and clinical studies that document typical distribution patterns in affected communities.

Because the system in Eqs. (1) involves the delayed terms $S(t-\tau)$ and $D(t-\tau)$, the problem must be supplemented with history functions on the interval $[-\tau, 0]$. We use constant histories taken equal to the prescribed initial values:

$$S(t) = 200, \quad D(t) = 70, \quad T(t) = 20, \quad R(t) = 20, \qquad -\tau \le t \le 0. \tag{2}$$

This choice models a community whose state has been approximately constant just before the time horizon of interest, and is therefore consistent with the static distribution patterns that motivated the initial values $S(0), D(0), T(0), R(0)$. The same constant histories are passed as the history argument to the MATLAB solvers `dde23` and `ddesd` when they are used for benchmarking in Section 4.2, so that the Taylor-wavelet method and the benchmark solvers solve exactly the same delay initial-value problem.

These initial conditions represent a community with established alcohol consumption patterns and limited treatment access. The distribution shows typical endemic alcohol problems: many heavy drinkers with small groups in treatment and recovery. This baseline lets us examine how interventions might change these proportions. All rate parameters given in Table 1 are expressed on a daily basis (day^{-1}), with the exception of the carrying capacity K, which is a population count. The parameter values are taken from Bouajaji et al. [4] and have not been calibrated against case data. Their numerical magnitudes should be interpreted as dimensionless rates rather than as values calibrated to a specific time unit; the horizon $T_f = 30$ should accordingly be read as a stylized epidemic time window rather than as a literal 30-day interval.

The system in Eqs. (1) admits the drinking-free equilibrium (DFE) $(S^*, D^*, T^*, R^*) = (K, 0, 0, 0) = (600, 0, 0, 0)$, which is verified by direct substitution into the four right-hand sides. The basic reproduction number R_0 for this model, including its dependence on the delay through the survival factor $e^{-\mu\tau}$, is derived in detail in Bouajaji et al. [4] via the next-generation-matrix construction; for the parameter values in Table 1 the system is in the parameter regime $R_0 > 1$, in which the DFE is unstable and the system approaches an endemic equilibrium on long time scales. Our numerical study takes place in this endemic regime and concerns the parameter dependence of the transient and late-phase dynamics rather than the existence or stability of the equilibria themselves.

3 The Taylor wavelet method and its implementation

In this section, we introduce the Taylor wavelet method and its implementation to the SDTR model.

3.1 The Taylor wavelet method

The generalized Taylor wavelets $\psi^h_{n,m}(t) = \psi(k, n, m, t)$ are defined over the interval $[0, h)$ and characterized by four parameters: $k \in \mathbb{N}$ denotes the level of resolution and determines the number of subintervals $J = 2^{k-1}$; $n = 1, 2, \ldots, 2^{k-1}$ indicates the translation index corresponding to a specific subinterval;

Table 1: Definition and values of model parameters

Parameter	Definition	Value
r_1	Intrinsic growth rate	0.2
K	Carrying capacity (population count)	600
β_1	Transmission coefficient (S to D)	0.03
β_2	Relapse coefficient (T to D)	0.03
α_1	Inhibitory effect in S	0.01
α_2	Inhibitory effect in D	0.02
η	Rate R to S	0.1
γ	Treatment entry rate	0.4
σ	Recovery rate in treatment	0.1
δ_1	Alcohol-related death rate (D)	0.35
δ_2	Alcohol-related death rate (T)	0.3
μ	Natural death rate	0.04
τ	Incubation period (stylized time units)	4

$m = 0, 1, \ldots, M-1$ represents the degree of the local Taylor polynomial; t is the time variable. The wavelet basis function is defined as

$$\psi_{n,m}^{h}(t) = \begin{cases} 2^{(k-1)/2}\, \tilde{T}_m\left(\dfrac{2^{k-1}t}{h} - n + 1\right), & \dfrac{(n-1)h}{2^{k-1}} \le t < \dfrac{nh}{2^{k-1}}, \\ 0, & \text{otherwise}, \end{cases} \tag{3}$$

where

$$\tilde{T}_m(t) = \sqrt{2m+1}\, t^m, \qquad m = 0, 1, \ldots, M-1, \tag{4}$$

is the monomial t^m rescaled so that $\int_0^1 \tilde{T}_m(t)^2\, dt = 1$. Under this scaling, the rescaled local variable $u = 2^{k-1}t/h - n + 1$ maps each subinterval $\left[(n-1)h/2^{k-1}, nh/2^{k-1}\right)$ onto $[0,1)$, on which the $\tilde{T}_m$ are individually L^2-unit-normalized; the prefactor $2^{(k-1)/2}$ then preserves the L^2-norm of each wavelet on the subinterval. We note that $\{\tilde{T}_m\}_{m\ge 0}$ are individually unit-normalized but not mutually orthogonal on $[0,1]$; the basis $\{\psi_{n,m}^{h}\}$ is therefore a Riesz basis of piecewise polynomials, not an orthonormal basis. Approximation in this basis remains stable because, on each subinterval, $\{1, t, \ldots, t^{M-1}\}$ is linearly independent and dense in $C[0, h/J]$ as $M \to \infty$. Taylor wavelets offer a flexible and localized basis for approximating functions with varying smoothness because of their polynomial structure.

3.2 Function approximation

Let $f(t)$ be a sufficiently smooth function defined over the interval $[0, h)$. The generalized Taylor wavelet expansion of $f(t)$ can be expressed as follows:

$$f(t) \approx \sum_{n=1}^{2^{k-1}} \sum_{m=0}^{M-1} c_{n,m}\, \psi_{n,m}^{h}(t), \tag{5}$$

where $\psi^h_{n,m}$ are the Taylor wavelet basis functions defined in Eq. (3) and $c_{n,m}$ are the unknown coefficients to be determined. We can rewrite Eq. (5) using matrix notation:

$$f(t) \approx \mathbf{c}^T \Psi(t), \tag{6}$$

where $\mathbf{c}$ and $\Psi(t)$ are the $2^{k-1}M \times 1$ vectors of unknown wavelet coefficients and basis functions, respectively.

The derivative of $f(t)$ can be obtained by differentiating Eq. (6):

$$\frac{df(t)}{dt} \approx \mathbf{c}^T \frac{d\Psi(t)}{dt}$$

and the derivative of the wavelet vector $\Psi(t)$ can be approximated by a linear combination of the basis functions themselves:

$$\frac{d\Psi(t)}{dt} \approx A\,\Psi(t),$$

where A is the $2^{k-1}M \times 2^{k-1}M$ operational matrix of differentiation.

Differentiating Eq. (3) on the n-th subinterval gives

$$\frac{d}{dt}\psi^h_{n,m}(t) = \frac{J}{T_f}\, m \sqrt{\frac{2m+1}{2m-1}}\, \psi^h_{n,m-1}(t), \qquad m \geq 1, \tag{7}$$

and zero for $m = 0$, where $J = 2^{k-1}$ and T_f is the simulation horizon. We use T_f for the simulation horizon to avoid notational clash with the treatment compartment $T(t)$. Consequently A is block-diagonal,

$$A = \mathrm{diag}(A_{\mathrm{loc}}, A_{\mathrm{loc}}, \ldots, A_{\mathrm{loc}}), \quad J \text{ blocks}, \tag{8}$$

where the local block $A_{\mathrm{loc}} \in \mathbb{R}^{M\times M}$ is lower-bidiagonal with entries

$$(A_{\mathrm{loc}})_{m,m-1} = \frac{J}{T_f}\, m \sqrt{\frac{2m+1}{2m-1}}, \quad m = 1, \ldots, M-1, \tag{9}$$

and all other entries zero. Written out in full:

$$A_{\mathrm{loc}} = \frac{J}{T_f} \begin{pmatrix} 0 & 0 & 0 & \cdots & 0 \\ 1\cdot\sqrt{\frac{3}{1}} & 0 & 0 & \cdots & 0 \\ 0 & 2\cdot\sqrt{\frac{5}{3}} & 0 & \cdots & 0 \\ 0 & 0 & 3\cdot\sqrt{\frac{7}{5}} & \cdots & 0 \\ \vdots & & & \ddots & \vdots \\ 0 & \cdots & 0 & (M-1)\sqrt{\frac{2M-1}{2M-3}} & 0 \end{pmatrix}. \tag{10}$$

The matrix A has $(M-1)J$ non-zero entries out of $(JM)^2$ total, so the fill fraction $(M-1)/(JM^2)$ decreases rapidly with increasing k or M, which contributes to the efficiency of the method. Hence, the derivative of $f(t)$ can be expressed as

$$\frac{df(t)}{dt} \approx \mathbf{c}^T A\,\Psi(t). \tag{11}$$

3.3 Convergence analysis

We establish an L^2 error bound for the Taylor-wavelet approximation on $[0,T_f]$, following the framework of Keshavarz et al. [13]. The collocation points are uniformly distributed on each subinterval of width $h = T_f/J$ with $J = 2^{k-1}$, so we base the analysis on the standard uniform-node interpolation error. Throughout this section, $h = T_f/J$ denotes the uniform subinterval width, which is distinct from the interval parameter h appearing in the wavelet definition of Section 3.1; since the wavelets are applied exclusively on $[0,T_f)$ in this work, the two usages do not conflict.

Theorem 1. *Let $f \in C^M[a,b]$ and let $S_{M-1}(x)$ be the polynomial of degree $M-1$ interpolating f at M uniformly spaced nodes on $[a,b]$. Then*

$$|f(x) - S_{M-1}(x)| \;\le\; \frac{(b-a)^M}{4M\,(M-1)^M} \max_{\xi\in[a,b]} \left|f^{(M)}(\xi)\right|, \tag{12}$$

for all $x \in [a,b]$.

This is the classical Cauchy-form error bound for equispaced Lagrange interpolation; see e.g. Atkinson [1].

Theorem 2. *Suppose $f \in C^M[0,T_f]$ and $f(x) \approx C^\top \Psi(x)$ is the Taylor-wavelet approximation of f on $[0,T_f]$ with $J = 2^{k-1}$ subintervals of width $h = T_f/J$ and uniform collocation nodes. Then*

$$\left\|f - C^\top \Psi\right\|_{L^2[0,T_f]} \le \frac{\sqrt{T_f}\,h^M}{4M\,(M-1)^M} \max_{\xi\in[0,T_f]} \left|f^{(M)}(\xi)\right|. \tag{13}$$

Proof. Partition $[0,T_f]$ into the $J = 2^{k-1}$ subintervals $I_{k,n} = \big[(n-1)h,\, nh\big]$, $n = 1,\dots,J$, each of width $h = T_f/J$. On each subinterval, $C^\top\Psi$ is the best L^2-approximation of f in the local polynomial space of degree $M-1$, so for the uniform-node interpolant S_{M-1} on $I_{k,n}$,

$$\int_{I_{k,n}} \big(f - C^\top\Psi\big)^2 dx \;\le\; \int_{I_{k,n}} \big(f - S_{M-1}\big)^2 dx.$$

Applying Theorem 1 on $I_{k,n}$ (interval length h),

$$\left|f(x) - S_{M-1}(x)\right| \;\le\; \frac{h^M}{4M(M-1)^M} \max_{\xi\in[0,T_f]} \left|f^{(M)}(\xi)\right| \;=:\; E,$$

so $\int_{I_{k,n}} (f - S_{M-1})^2\,dx \le hE^2$. Summing over the J subintervals,

$$\|f - C^\top\Psi\|^2_{L^2[0,T_f]} \;\le\; JhE^2 \;=\; T_f E^2,$$

since $Jh = T_f$. Taking square roots gives (13). □

The bound (13) reveals two convergence mechanisms. First, fixing k and increasing M, the factor $h^M/[4M(M-1)^M]$ decays super-algebraically in M, since $h/(M-1) < 1$ for the parameters used here. Second, fixing M and increasing k, the subinterval width $h = T_f/2^{k-1}$ halves per level, so the bound decreases by a factor of 2^M per increment of k.

It is important to note that Theorem 2 is an approximation-theoretic result. It quantifies how well a sufficiently smooth function can be represented in the Taylor wavelet basis, but does not establish convergence of the collocation solution to the true solution of the nonlinear DDE system (1). A rigorous convergence analysis of the collocation scheme would additionally require stability estimates for the nonlinear iteration and consistency estimates for the delay operator, which lie beyond the scope of the present work.

3.4 Application to the SDTR model

The Taylor wavelet method is applied directly to the system of DDEs in Eq. (1). First, we approximate each state variable and its derivative using the wavelet series and the operational matrix of differentiation as in Eqs. (6) and (11):

$$S(t) \approx \mathbf{s}^T\Psi(t), \quad D(t) \approx \mathbf{d}^T\Psi(t), \quad T(t) \approx \mathbf{q}^T\Psi(t), \quad R(t) \approx \mathbf{r}^T\Psi(t),$$
$$\frac{dS(t)}{dt} \approx \mathbf{s}^T A\Psi(t), \quad \frac{dD(t)}{dt} \approx \mathbf{d}^T A\Psi(t), \quad \frac{dT(t)}{dt} \approx \mathbf{q}^T A\Psi(t), \quad \frac{dR(t)}{dt} \approx \mathbf{r}^T A\Psi(t),$$

where $\mathbf{s}, \mathbf{d}, \mathbf{q}$ and $\mathbf{r}$ are the unknown coefficient vectors to be determined.

By substituting these approximations into Eq. (1) and moving the right-hand sides to the left, we obtain the algebraic system

$$\mathbf{s}^T A\Psi(t) - r_1\left(1 - \tfrac{N(t)}{K}\right)N(t) + \tfrac{\beta_1 \mathbf{s}^T\Psi(t)\,\mathbf{d}^T\Psi(t)}{1+\alpha_1 \mathbf{s}^T\Psi(t)+\alpha_2 \mathbf{d}^T\Psi(t)} - \eta\,\mathbf{r}^T\Psi(t) \approx \mathbf{0},$$
$$\mathbf{d}^T A\Psi(t) - e^{-\mu\tau}\tfrac{\beta_1 \mathbf{s}^T\Psi(t-\tau)\,\mathbf{d}^T\Psi(t-\tau)}{1+\alpha_1 \mathbf{s}^T\Psi(t-\tau)+\alpha_2 \mathbf{d}^T\Psi(t-\tau)} - \beta_2\,\mathbf{q}^T\Psi(t)\,\mathbf{d}^T\Psi(t) + (\mu+\delta_1+\gamma)\,\mathbf{d}^T\Psi(t) \approx \mathbf{0},$$
$$\mathbf{q}^T A\Psi(t) - \gamma\mathbf{d}^T\Psi(t) + \beta_2\,\mathbf{q}^T\Psi(t)\,\mathbf{d}^T\Psi(t) + (\mu+\delta_2+\sigma)\,\mathbf{q}^T\Psi(t) \approx \mathbf{0},$$
$$\mathbf{r}^T A\Psi(t) - \sigma\,\mathbf{q}^T\Psi(t) + (\mu+\eta)\,\mathbf{r}^T\Psi(t) \approx \mathbf{0}.$$

The residual functions defined in Section 4.1 are derived from the same sign convention as the system above; the residual values reported in Tables 2–3 therefore correspond to this corrected algebraic system.

We now make the discretization explicit. The wavelet expansion in Eq. (3) is defined only for $t \geq 0$, so the delayed values must be supplied by the history ϕ for $t-\tau < 0$. Writing ϕ_S, ϕ_D for the corresponding constant histories given in Eq. (2), we set

$$\widehat{S}(t-\tau) = \begin{cases} \phi_S, & t-\tau < 0, \\ \mathbf{s}^T\Psi(t-\tau), & t-\tau \geq 0, \end{cases} \qquad \widehat{D}(t-\tau) = \begin{cases} \phi_D, & t-\tau < 0, \\ \mathbf{d}^T\Psi(t-\tau), & t-\tau \geq 0, \end{cases} \tag{14}$$

and substitute $\widehat{S}(t-\tau), \widehat{D}(t-\tau)$ for $S(t-\tau), D(t-\tau)$ in the delayed incidence term of the D-equation. Because the initial-condition constraints below force $\mathbf{s}^T\Psi(0) = \phi_S$ and $\mathbf{d}^T\Psi(0) = \phi_D$, the substitution is continuous at $t = \tau$.

The residual equations are collocated on the uniform grid $t_j = jT_f/[J(M-1)]$, $j = 1, \ldots, J(M-1)$, contributing $J(M-1)$ equations per compartment. The initial conditions $\mathbf{s}^T\Psi(0) = 200$, $\mathbf{d}^T\Psi(0) = 70$, $\mathbf{q}^T\Psi(0) = 20$, $\mathbf{r}^T\Psi(0) = 20$ contribute one more equation per compartment. Continuity of each compartment at every interior breakpoint $\xi_\ell = \ell T_f/J$ (for $\ell = 1, \ldots, J-1$) is also enforced, contributing $J-1$ additional equations per compartment. Together, this yields a square nonlinear system of $4JM$ equations

for the $4JM$ unknowns, which is solved with the MATLAB routine `fsolve` (default function tolerance 10^{-6}, step tolerance 10^{-10}). Once the coefficient vectors are recovered, continuous approximations for $S(t), D(t), T(t), R(t)$ are obtained.

4 Error analysis and method accuracy

Since an analytical solution for the nonlinear DDE system in Eq. (1) does not exist, we establish the accuracy and reliability of the proposed Taylor wavelet method (TWM) through residual error analysis and comparison with established high-precision numerical methods.

4.1 Residual error analysis

The residual error shows how well an approximate solution satisfies the differential equation. Lower residual values indicate better accuracy. Let us denote the approximate solutions by $\tilde{S}(t), \tilde{D}(t), \tilde{T}(t)$, and $\tilde{R}(t)$. We obtain the residual functions by substituting these approximate solutions back into the governing system of Eqs. (1) as follows:

$$
\begin{aligned}
Res_S(t) &= \frac{d\tilde{S}(t)}{dt} - \left[r_1 \left(1 - \frac{N(t)}{K}\right) N(t) - \frac{\beta_1 \tilde{S}(t)\tilde{D}(t)}{1+\alpha_1 \tilde{S}(t)+\alpha_2 \tilde{D}(t)} + \eta \tilde{R}(t) \right], \\
Res_D(t) &= \frac{d\tilde{D}(t)}{dt} - \left[e^{-\mu\tau} \frac{\beta_1 \tilde{S}(t-\tau)\tilde{D}(t-\tau)}{1+\alpha_1 \tilde{S}(t-\tau)+\alpha_2 \tilde{D}(t-\tau)} + \beta_2 \tilde{T}(t)\tilde{D}(t) - (\mu+\delta_1+\gamma)\tilde{D}(t) \right], \\
Res_T(t) &= \frac{d\tilde{T}(t)}{dt} - \left[\gamma \tilde{D}(t) - \beta_2 \tilde{T}(t)\tilde{D}(t) - (\mu+\delta_2+\sigma)\tilde{T}(t) \right], \\
Res_R(t) &= \frac{d\tilde{R}(t)}{dt} - \left[\sigma \tilde{T}(t) - (\mu+\eta)\tilde{R}(t) \right].
\end{aligned}
$$

We calculate the maximum residual error for different values of the resolution parameter k and the degree of the polynomial M to quantify the overall error throughout the simulation interval $[0, T_f]$. The results of this analysis are presented in Tables 2 and 3.

Table 2 shows the residual errors for different values of the resolution parameter k while keeping the degree of the polynomial fixed at $M = 8$. We observe that increasing k from 1 to 4 decreases the maximum residual error in all compartments and improves the accuracy by several orders of magnitude. This shows an advantage of the wavelet method: we can improve precision by increasing the resolution parameter (k) without increasing the degree of the polynomial approximation (M). Since we obtain the lowest error at $k = 4$, we fix this number throughout the study.

Now, we decide the degree of the polynomial. Table 3 presents the residual error for a fixed resolution level ($k = 4$) while varying the degree of the approximation polynomial (M). As anticipated, increasing the degree of the polynomial from $M = 4$ to $M = 10$ also results in a dramatic reduction in residual error, showing good convergence of the method as we increase the polynomial degree. We observe that taking $M = 8$ is sufficient to obtain highly accurate results in all compartments.

These results show that a configuration of $k = 4$ and $M = 8$ results in very low residual errors on the order of $\mathcal{O}(10^{-12})$ or smaller for all compartments. This confirms the accuracy of the Taylor wavelet method and shows that it is reliable for subsequent parametric analysis. Tables 2–3 show empirical convergence in both k and M, consistent with the theoretical bound established in Theorem 2.

Table 2: Maximum residual errors for different values of k when $M = 8$

Level of resolution	$S(t)$	$D(t)$	$T(t)$	$R(t)$
$k = 1$	7.4585×10^{-5}	3.5325×10^{-4}	3.5312×10^{-4}	7.8642×10^{-9}
$k = 2$	2.1922×10^{-8}	8.0919×10^{-7}	8.1646×10^{-7}	1.4519×10^{-8}
$k = 3$	2.1981×10^{-10}	1.8107×10^{-9}	1.8162×10^{-9}	1.1112×10^{-11}
$k = 4$	5.6559×10^{-12}	1.0374×10^{-12}	5.9277×10^{-12}	2.3981×10^{-14}

Table 3: Maximum residual errors for different degrees of polynomials when $k = 4$

Degree of polynomial	$S(t)$	$D(t)$	$T(t)$	$R(t)$
$M = 4$	4.6918×10^{-6}	1.5335×10^{-5}	1.5331×10^{-5}	1.3908×10^{-7}
$M = 6$	6.2785×10^{-10}	1.5727×10^{-9}	1.5750×10^{-9}	5.4205×10^{-11}
$M = 8$	5.6559×10^{-12}	1.0374×10^{-12}	5.9277×10^{-12}	2.3981×10^{-14}
$M = 10$	3.9933×10^{-12}	1.7479×10^{-12}	4.8994×10^{-13}	1.0658×10^{-14}

4.2 Comparison with benchmark methods

We also compare the solutions obtained from the TWM with two established and widely accepted numerical solvers for delay differential equations, namely `dde23` and `ddesd`, to further validate our results. `dde23` is based on the Runge–Kutta method, specifically adapted to handle delay differential equations. `ddesd` is MATLAB's solver for problems where the delay itself depends on the state or time; it employs a variable-step, variable-order method and is included here as a high-precision benchmark because its adaptive scheme is generally more conservative than `dde23` for stiff or sensitive delay systems.

Tables 4–7 present the numerical results obtained by the TWM, `dde23` and `ddesd` for each of the four state variables at various time points. One can see that the TWM achieves excellent agreement with both benchmark methods. The TWM solution agrees with `dde23` to 7–8 significant digits and with `ddesd` to 8–10 significant digits; since both reference solutions are themselves numerical, this is a mutual-consistency check rather than a comparison with a closed-form reference. These results show that TWM is reliable and captures the system dynamics.

Table 4: Numerical results obtained by the TWM, `dde23` and `ddesd` for $S(t)$ at different times

t	TWM	`dde23`	`ddesd`
0.2	186.546548468787	186.546548575608	186.546548456702
0.4	172.192288873300	172.192288950454	172.192288838948
0.6	157.649356777545	157.649356830669	157.649356714367
0.8	143.409870157904	143.409870174847	143.409870073269
1.0	129.808059720952	129.808059717840	129.808059629883

Figure 2 overlays the TWM solution and the `dde23` reference for all four compartments on the full

Table 5: Numerical results obtained by the TWM, `dde23` and `ddesd` for $D(t)$ at different times

t	TWM	`dde23`	`ddesd`
0.2	82.4287422089702	82.4287424782076	82.4287422057971
0.4	92.7577525882864	92.7577528693256	92.7577525407125
0.6	101.4713623355570	101.4713625855180	101.4713622954430
0.8	109.0102916554720	109.0102918840220	109.0102916491880
1.0	115.6930331586670	115.6930333648550	115.6930331693230

Table 6: Numerical results obtained by the TWM, `dde23` and `ddesd` for $T(t)$ at different times

t	TWM	`dde23`	`ddesd`
0.2	16.2949654573352	16.2949651936260	16.2949654690468
0.4	14.0632073775754	14.0632071182346	14.0632074494141
0.6	12.8553845492185	12.8553843280412	12.8553846189643
0.8	12.2673633654968	12.2673631787139	12.2673634122421
1.0	12.0177964548175	12.0177962958319	12.0177964875697

Table 7: Numerical results obtained by the TWM, `dde23` and `ddesd` for $R(t)$ at different times

t	TWM	`dde23`	`ddesd`
0.2	19.8027718547877	19.8027718657409	19.8027718543824
0.4	19.5531905214575	19.5531905315822	19.5531905195128
0.6	19.2773747081677	19.2773747167352	19.2773747055440
0.8	18.9920618370140	18.9920618439320	18.9920618345391
1.0	18.7067433731348	18.7067433789589	18.7067433708239

simulation interval $[0,30]$. The two solutions are visually indistinguishable across the entire horizon.

5 Numerical simulations

In this section, we first analyze the dynamics of the system with the given parameter values. Then we explore the effects of the model parameters on the system by varying one parameter at a time while keeping other parameters fixed. The aim is to understand the most important parameters that change the dynamics of the system and to discuss public health implications.

5.1 Analysis of the population dynamics

Figure 2 presents the evolution of the susceptible (S), heavy drinker (D), treatment (T) and recovered (R) populations over 30 time units. This interval captures the short-term outbreak dynamics of the system,

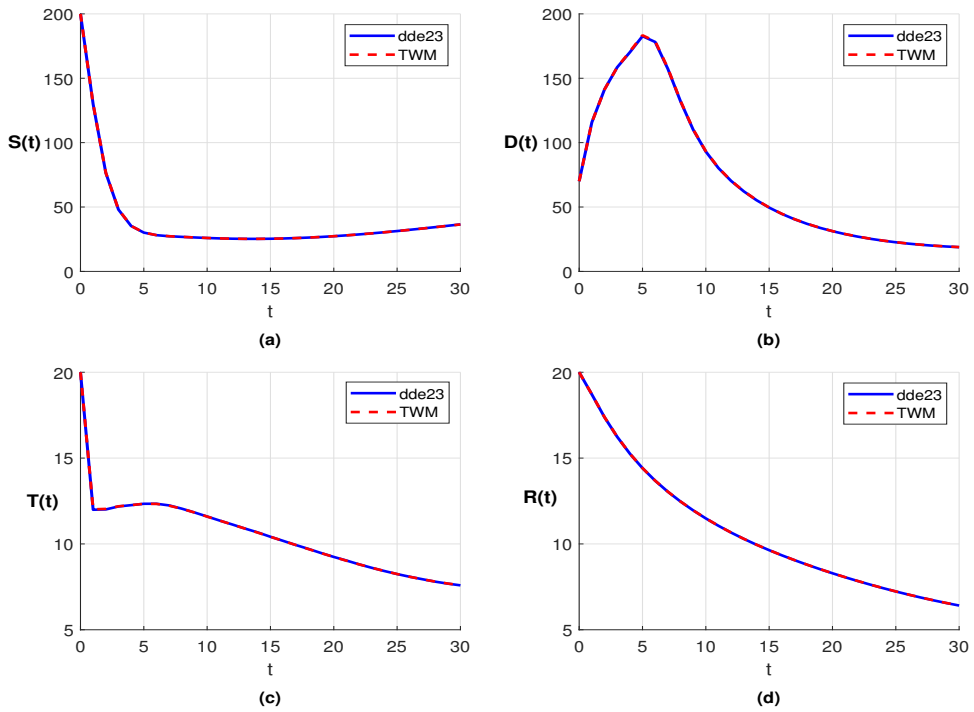

Figure 2: Comparison of the Taylor wavelet method (TWM, red dashed) with the MATLAB `dde23` solver (blue solid) on the full simulation interval $[0,30]$, for the four compartments $S(t), D(t), T(t), R(t)$

including the epidemic peak and the initial approach to a stable regime.

Figure 2(a) presents the behavior of the S population consisting of moderate and occasional drinkers with a population size of 200. One can see that this group experiences a significant decline during the first five time units, then stabilizes around 35 individuals. The main reason for this rapid depletion is the negative effect of the heavy drinker (D) group. Once they socialize, the S group increases their level of alcohol consumption and joins the D group. The constant recruitment into the S population is not enough to counteract this strong negative effect. This indicates that the social interaction with the D group is a dominant force in the system's dynamics.

Figure 2(b) shows the dynamic behavior of the heavy drinker population (D). This group initially has 70 individuals. As we already explained in Figure 2(a), they have a negative effect on the S group. Hence, the population of D increases and reaches a peak of more than 180 individuals at approximately 6 time units. After reaching its maximum, the population begins to decline as a portion of this group enrolls treatment centers, a portion dies due to natural or alcohol-related reasons. The heavy drinker group eventually settles at 20 individuals.

Figure 2(c) represents the dynamics of the treatment population (T). This group starts at 20 individuals and shows an initial sharp decline. This decrease has several reasons. Once they have contact with heavy drinkers, they relapse into heavy drinking and join the D group. Some individuals die naturally, while others die for alcohol-related reasons, which means it is too late for them to join the treatment center. The number of people in this population increases slightly around the fifth time unit due to tran-

sition from the D group. However, this increase is not enough to stabilize the population at that level. It continues to decrease and stabilizes around 7 individuals.

Figure 2(d) presents the behavior of the recovered population (R). This group begins with 20 individuals and experiences a decrease throughout the simulation. The population stabilizes at approximately 7 individuals. Although treated people join this group, the population continues to decrease. This is caused by two reasons: some people in the R group die naturally and leave the group, some begin to drink occasionally and transition to the S group.

5.2 Parametric sensitivity analysis using normalized sensitivity coefficients

We analyze how system dynamics depend on model parameters by varying each parameter individually keeping all other parameters at their baseline values. For each parameter configuration, the compartment trajectories were obtained by evaluating the continuous Taylor-wavelet polynomial approximation on a dense uniform grid over $[0, T_f]$. The peak value of each compartment and its corresponding time were identified as the discrete maximum over this grid; late-phase values at $t = 30$ were read as the final point of the same output. This provides a means to identify which factors play the largest role in public health outcomes. This one-at-a-time (OAT) approach is the standard local sensitivity protocol; it does not capture parameter interactions, which can in principle be substantial for delay systems with saturated incidence. The qualitative classification of parameters reported below should therefore be read as a local statement at the baseline. The normalized sensitivity coefficient for a state variable $X(t)$ with respect to parameter p is:

$$S_{p,X}(t) = \frac{\partial X(t)}{\partial p} \cdot \frac{p}{X(t)},$$

which represents the percentage change in $X(t)$ when parameter p changes by one percent.

We approximate this derivative by two-sided finite-range secant using two perturbed solutions $X(t; p_{\text{lo}})$ and $X(t; p_{\text{hi}})$:

$$S_{p,X}(t) \approx \frac{X(t, p_{\text{hi}}) - X(t, p_{\text{lo}})}{p_{\text{hi}} - p_{\text{lo}}} \cdot \frac{p}{X(t, p)}.$$

The perturbation values p_{lo} and p_{hi} for each parameter are listed in Table 8. They span the same biologically plausible range that we use in Figures 3–9, so that the sensitivity coefficients and the parameter-effect plots are based on the same numerical experiments.

Table 8: Perturbation values used for the two-sided finite-range secant sensitivity computation

Parameter	p_{lo}	p_0	p_{hi}
β_1	0.02	0.03	0.04
α_1	0.005	0.01	0.02
α_2	0.01	0.02	0.04
γ	0.3	0.4	0.5
σ	0.05	0.1	0.2
β_2	0.02	0.03	0.04
τ	0	4	8

We report the sensitivity coefficients at two characteristic times: $t = 5$ days, near the heavy drinker peak under baseline parameters; and $t = 30$ days, a late-time observation point. Figures 3–9 illustrate the system's dynamic behavior considering variations in parameters.

Table 9: Normalized sensitivity coefficients at peak ($t = 5$ days)

Parameter	$S_{p,S}$	$S_{p,D}$	$S_{p,T}$	$S_{p,R}$
β_1	−2.4490	0.9765	0.0829	0.0204
α_1	0.4236	−0.3698	−0.0321	−0.0082
α_2	1.1455	−0.3123	−0.0254	−0.0059
γ	0.0542	−0.0884	0.9934	0.2853
σ	0.0203	−0.0140	−0.0180	0.3029
β_2	−0.0562	0.0912	−1.0099	−0.2889
τ	0.0149	0.1193	0.0141	−0.0005

Table 10: Normalized sensitivity coefficients at late phase ($t = 30$ days)

Parameter	$S_{p,S}$	$S_{p,D}$	$S_{p,T}$	$S_{p,R}$
β_1	−2.0148	−0.8059	−0.2922	−0.1427
α_1	0.3979	0.0566	0.0210	0.0076
α_2	0.3403	0.3828	0.1428	0.0804
γ	0.5728	−0.0611	0.9647	0.9038
σ	0.1199	0.1867	−0.0236	0.8928
β_2	−0.3522	−0.0632	−0.6238	−0.6589
τ	−0.0096	−0.1000	−0.0236	0.0384

Tables 9 and 10 present a significant pattern: some parameters show contrasting dynamics at peak versus the late phase, while others preserve similar effects in both phases. We analyze these patterns by classifying parameters according to their temporal characteristics rather than discussing each individually.

Transmission and inhibition parameters

The most dramatic temporal variation appears in transmission coefficient β_1 and inhibition parameters α_1, α_2. Figure 3 shows that varying β_1 from 0.02 to 0.04 nearly doubles the heavy drinker peak (from 124 to 240 individuals) and accelerates peak timing from day 6 to day 5. Yet at the late phase ($t = 30$), all scenarios converge to similar levels around 18–26 individuals. The susceptible population behaves oppositely—it experiences permanent depletion, dropping from 200 to 17 individuals at the highest transmission rate.

The sensitivity coefficients confirm this temporal divergence. At peak, $S^{\text{peak}}_{\beta_1,D} = 0.9765$ indicates strong positive sensitivity—transmission directly amplifies outbreak severity. However, at the late phase the sign reverses: $S^{\text{ss}}_{\beta_1,D} = -0.8059$. The susceptible compartment shows the largest sensitivity magnitude

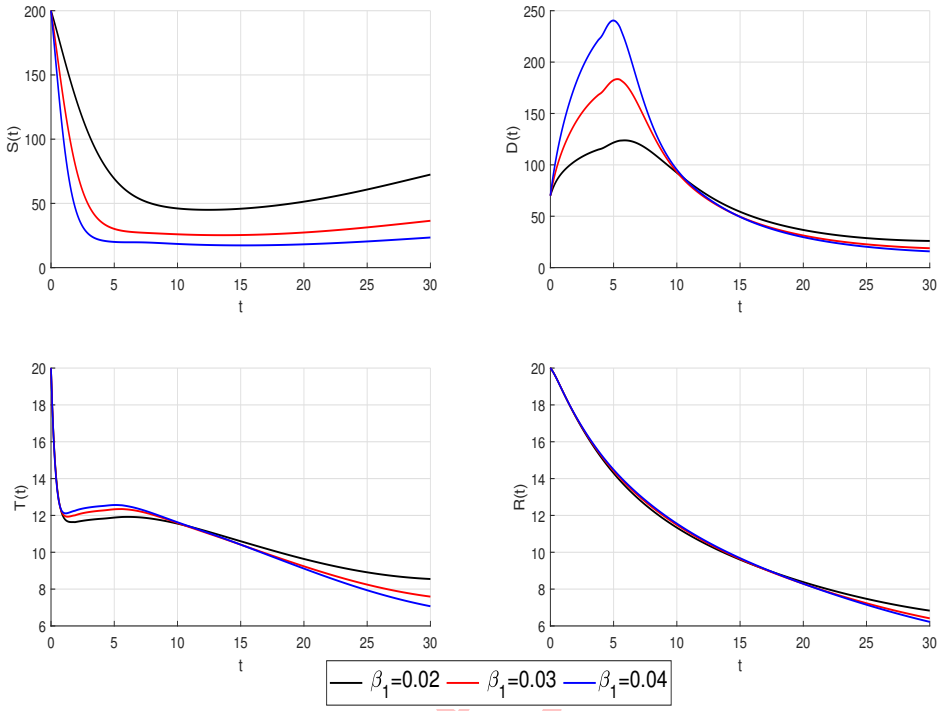

Figure 3: Parameter effect of β_1 on $S(t)$, $D(t)$, $T(t)$, $R(t)$

in the entire analysis: $S^{ss}_{\beta_1,S} = -2.0148$, reflecting permanent pool depletion. Treatment and recovery remain largely unaffected: $S^{ss}_{\beta_1,T} = -0.2922$ and $S^{ss}_{\beta_1,R} = -0.1427$.

The inhibitory parameters α_1 and α_2 follow similar temporal patterns but with opposite signs. Figures 4 and 5 demonstrate that increasing either parameter reduces peak burden substantially. For α_1, the peak drops from 229 to 134 individuals (43% reduction) while also delaying peak occurrence from day 5 to day 7. Parameter α_2 produces comparable reductions (220 to 140 individuals, 36% decrease). However, both parameters show convergence after day 15–20, with late-phase levels barely affected.

The sensitivity coefficients show this transient effectiveness. For α_1: peak sensitivity reaches $S^{peak}_{\alpha_1,D} = -0.3698$ but diminishes to $S^{ss}_{\alpha_1,D} = 0.0566$ at the late phase. Parameter α_2 shows similar decay from $S^{peak}_{\alpha_2,D} = -0.3123$ to $S^{ss}_{\alpha_2,D} = 0.3828$. Interestingly, α_2 produces a counterintuitive effect on susceptibles—higher inhibition preserves more susceptibles at the late phase (16, 28, and 50 individuals for increasing α_2), suggesting complex rebalancing dynamics where heavy drinker suppression paradoxically maintains a larger susceptible pool.

These three parameters share a critical characteristic: they control peak burden effectively but exert minimal influence on late-phase addiction levels. The difference between managing 125 versus 235 cases during the outbreak can determine healthcare system capacity. However, sustained addiction prevalence after 3–4 weeks depends on other factors entirely.

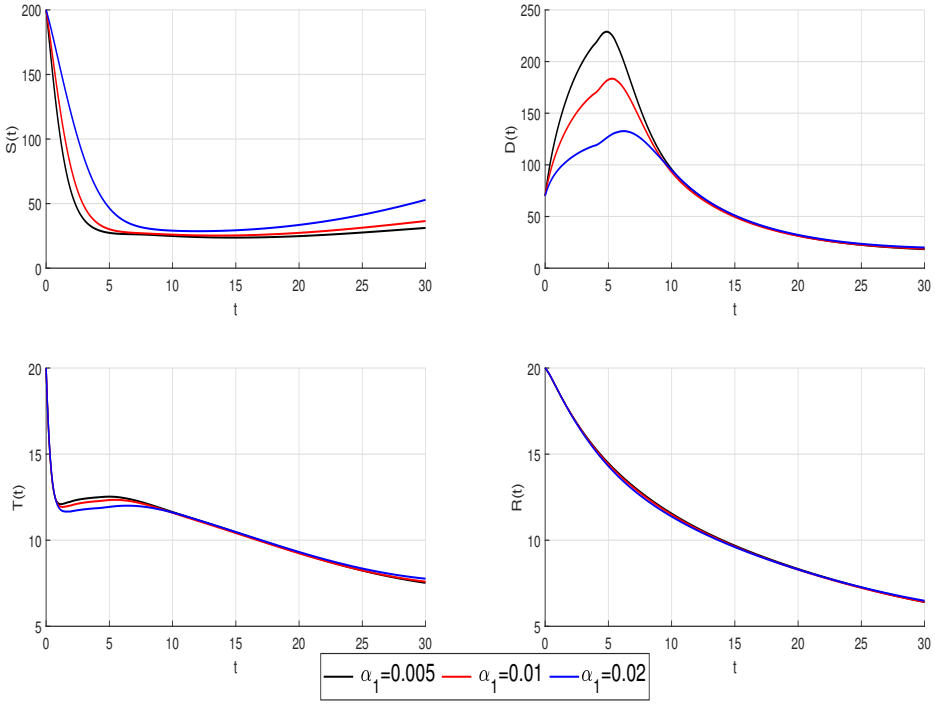

Figure 4: Parameter effect of α_1 on $S(t)$, $D(t)$, $T(t)$, $R(t)$

Treatment infrastructure parameters

Treatment entry rate γ and recovery rate σ behave very differently from transmission parameters. Instead of showing temporal divergence, they maintain consistent strong effects from outbreak through the late phase. Figure 6 shows that increasing γ from 0.3 to 0.5 produces separated trajectories that never converge. At the late phase, treatment population increases 64% (from 5.7 to 9.4 individuals), recovered population grows from 4.9 to 7.8, and heavy drinkers decrease from 19.2 to 18.6.

The sensitivity coefficients remain near unity across both phases: $S_{\gamma,T}^{\text{peak}} = 0.9934$ and $S_{\gamma,T}^{\text{ss}} = 0.9647$ for treatment population; $S_{\gamma,R}^{\text{ss}} = 0.9038$ for recovery. This shows a direct, proportional relationship—10% improvement in treatment access produces approximately 10% improvement in treatment and recovery outcomes, regardless of epidemic phase.

Recovery rate σ shows an interesting contrast: a small effect at the peak but a strong effect at the late phase. Figure 7 demonstrates that all recovery rate scenarios follow nearly identical paths during the early outbreak (peaks around 181–185 individuals). The difference emerges only at the late phase, where increasing σ from 0.05 to 0.2 grows the recovered population from 3.4 to 12.0 individuals (252% increase). The treatment population changes minimally (7.7 to 7.4) because patients complete treatment faster rather than accumulating.

The sensitivities show this delayed but cumulative impact. At the peak, the effect of σ on D and T is negligible ($S_{\sigma,D}^{\text{peak}} = -0.0140$, $S_{\sigma,T}^{\text{peak}} = -0.0180$), and the effect on R is moderate and positive ($S_{\sigma,R}^{\text{peak}} = 0.3029$). At the late phase, the effect on R becomes strong: $S_{\sigma,R}^{\text{ss}} = 0.8928$. This late-phase value nearly

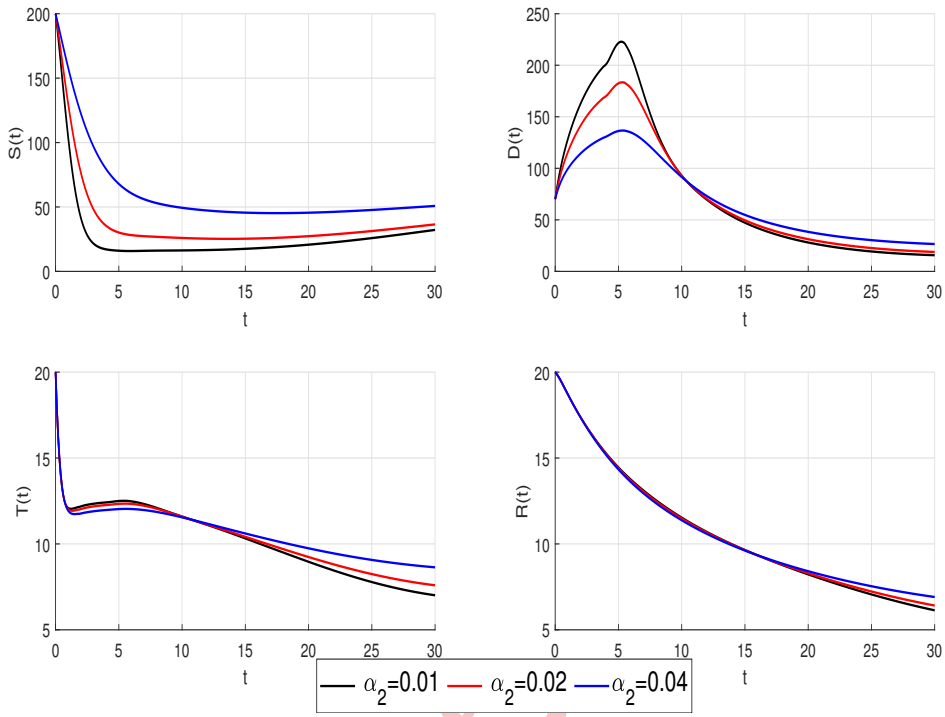

Figure 5: Parameter effect of α_2 on $S(t)$, $D(t)$, $T(t)$, $R(t)$

equals $S^{ss}_{\gamma,R} = 0.9038$, which means treatment quality and access contribute about equally to recovery outcomes. Improving recovery rates by 10% produces the same population-level benefit as expanding treatment capacity by 10%.

Relapse parameter

Relapse coefficient β_2 shows a different temporal pattern—strong negative effects that start immediately and accumulate continuously without convergence. Figure 8 shows that increasing β_2 from 0.02 to 0.04 causes persistent separation across all compartments. Treatment population drops 33% (9.5 to 6.4 individuals), recovered population decreases from 8.1 to 5.3, and heavy drinker peaks increase from 176 to 187. Unlike inhibition parameters where curves eventually reconverge, relapse damage is permanent.

Both peak and late-phase sensitivities show substantial magnitudes: $S^{peak}_{\beta_2,T} = -1.0099$ and $S^{ss}_{\beta_2,T} = -0.6238$ for treatment; $S^{ss}_{\beta_2,R} = -0.6589$ for recovery. The similarity between peak and late-phase values indicates relapse effects initiate immediately rather than building gradually. A 10% increase in relapse rates reduces treatment and recovery populations by approximately 6% permanently.

Time delay parameter

Unlike the other parameters, τ produces a non-monotonic response in every compartment over the plausible range $\tau \in [0, 8]$. Figure 9 shows that increasing τ from 0 to 8 days shifts peak timing from day 2 to

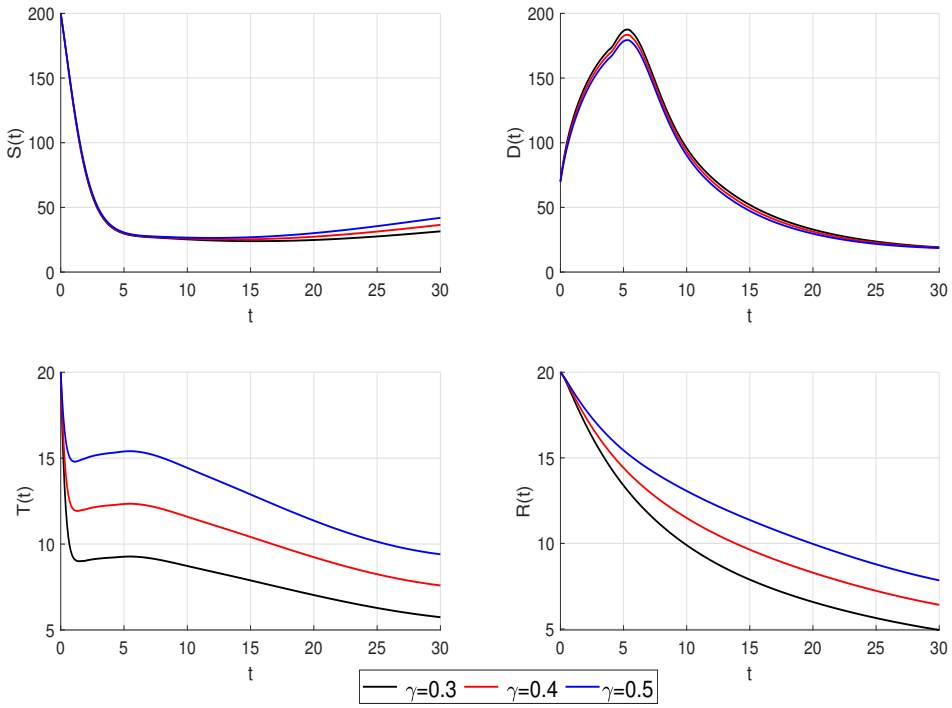

Figure 6: Parameter effect of γ on $S(t)$, $D(t)$, $T(t)$, $R(t)$

Table 11: Compartment values across the τ-sweep

τ	D_{peak}	t^*	$S(t=30)$	$D(t=30)$	$T(t=30)$	$R(t=30)$
0	158.49	2.05	32.92	24.99	8.39	6.38
1	173.95	2.95	35.14	22.90	8.11	6.28
2	186.14	3.75	36.70	20.61	7.79	6.28
3.6	184.06	4.95	36.77	18.97	7.59	6.37
4	183.64	5.31	36.50	18.82	7.59	6.41
4.4	181.61	5.65	36.03	18.89	7.61	6.46
6	176.22	7.10	34.49	19.36	7.73	6.63
8	163.91	8.95	32.21	21.22	8.04	6.87

day 9 and changes peak magnitude in a non-monotonic way: D_{peak} rises from 158 at $\tau = 0$ to a maximum of 183 near $\tau = 4$, then declines to 164 at $\tau = 8$.

To investigate this behavior, we extend the analysis with a finer τ-sweep, reported in Table 11.

Each compartment has an interior extremum: D_{peak} attains a maximum near $\tau \approx 2$–3, $S(t=30)$ a maximum near $\tau \approx 3.6$, and $D(t=30)$, $T(t=30)$ reach a minimum near $\tau \approx 4$. The peak time t^* increases nearly linearly with τ.

Because the baseline $\tau = 4$ lies close to these extrema, the local sensitivities at $\tau = 4$, computed with

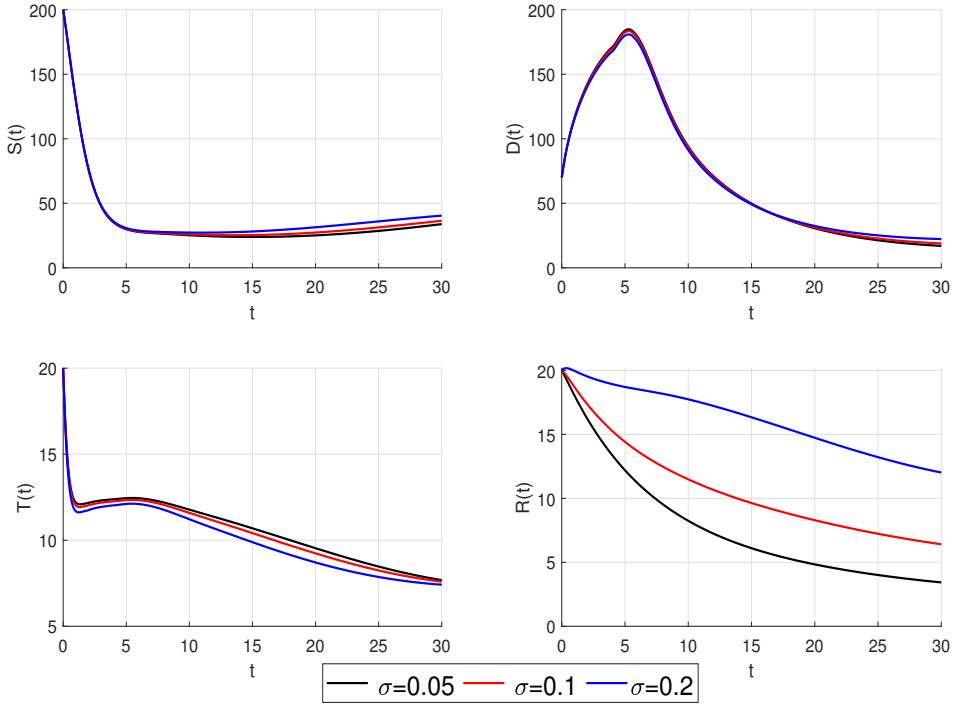

Figure 7: Parameter effect of σ on $S(t)$, $D(t)$, $T(t)$, $R(t)$

Table 12: Local sensitivity coefficients at $\tau = 4$, computed with $\tau \in \{3.6, 4.4\}$

Time	$S_{\tau,S}$	$S_{\tau,D}$	$S_{\tau,T}$	$S_{\tau,R}$
$t = 5$	0.0333	-0.1880	-0.0185	-0.0038
$t = 30$	-0.1004	-0.0225	0.0109	0.0711

the closer values $\tau \in \{3.6, 4.4\}$, are small for every compartment. We note that the global two-sided finite-range secant over $\tau \in \{0, 8\}$ reported in Table 9 ($S^{\text{peak}}_{\tau,D} = +0.1193$) captures the overall shape of $D(5;\tau)$ across the full plausible range and hence returns a positive value; the local sensitivity at $\tau = 4$ in Table 12 ($S^{\text{peak}}_{\tau,D} = -0.1880$) uses a narrow perturbation $\tau \in \{3.6, 4.4\}$ and captures the local slope, which is negative because $\tau = 4$ lies just past the peak of $D_{\text{peak}}(\tau)$. Both quantities are informative but measure different aspects of the delay response. These local values are reported in Table 12.

6 Conclusion

We solved a nonlinear delayed alcoholism model using the Taylor wavelet method and analyzed parameter sensitivity at epidemic peaks and at the late phase of the simulation. The method gives residual errors around $\mathcal{O}(10^{-12})$ and matches benchmark solvers to 7–10 decimal places.

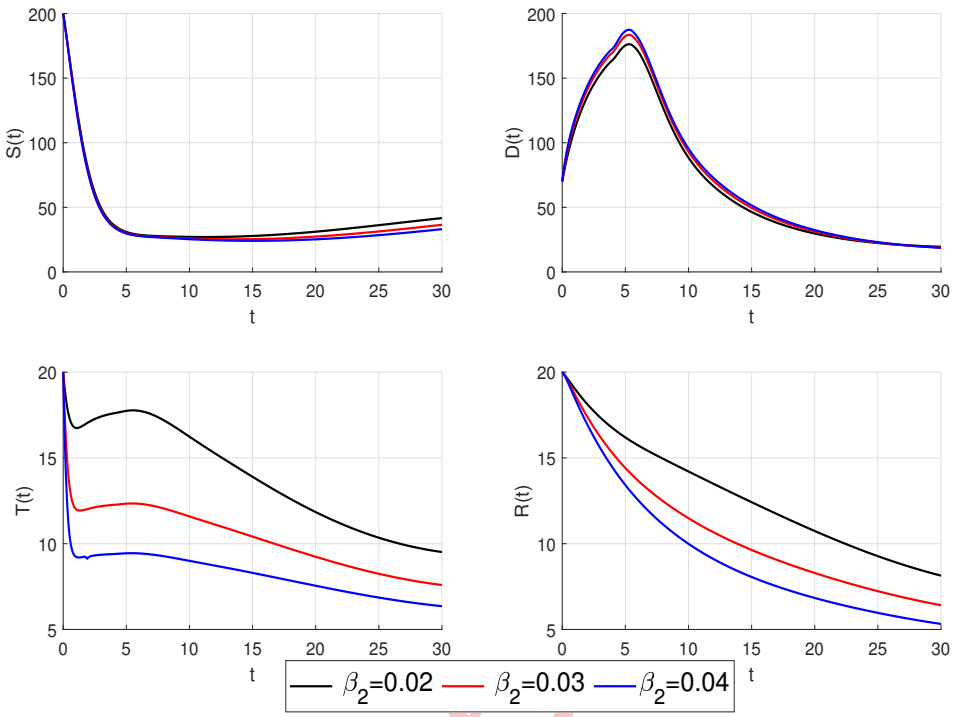

Figure 8: Parameter effect of β_2 on $S(t)$, $D(t)$, $T(t)$, $R(t)$

The main finding is that parameters behave very differently at peaks versus the late phase. Transmission (β_1) and inhibition (α_1, α_2) have high peak sensitivity but minimal late-phase effects. Social transmission sensitivity is $S^{\text{peak}}_{\beta_1,D} = 0.98$ at peak but reverses to $S^{\text{ss}}_{\beta_1,D} = -0.81$ at the late phase. Inhibitory parameters cut peaks by 40–60% but barely affect late-phase levels.

Treatment parameters work oppositely—they have strong effects at the late phase, while γ also acts strongly at peak. Treatment entry and recovery rate both show sensitivities near 0.9 at the late phase ($S^{\text{ss}}_{\gamma,T} = 0.96$, $S^{\text{ss}}_{\sigma,R} = 0.89$), meaning treatment quality and access matter equally for recovery. Relapse has strong negative effects at both phases ($S^{\text{ss}}_{\beta_2,T} = -0.62$, $S^{\text{ss}}_{\beta_2,R} = -0.66$), with damage that accumulates permanently.

The time delay τ produces a non-monotonic response in every compartment over $\tau \in [0,8]$: each compartment has an interior extremum, with D_{peak} maximized near $\tau \approx 2$–3 and $D(t=30)$ minimized near $\tau \approx 4$. Local sensitivities at the baseline $\tau = 4$ are small in magnitude ($|S_{\tau,X}| < 0.20$ for every compartment).

These temporal differences mean we need different strategies for different goals. For managing peaks and reducing healthcare burden, target social transmission through awareness campaigns and peer support programs. These reduce peak loads substantially but will not change long-term addiction levels. For reducing late-phase addiction levels, sustained investment in treatment infrastructure is needed—both capacity and quality matter equally.

Sustained relapse prevention is an important component of any control strategy, since the magnitudes $|S^{\text{ss}}_{\beta_2,T}|, |S^{\text{ss}}_{\beta_2,R}| \approx 0.6$ indicate that reducing relapse delivers a benefit comparable to expanding treatment

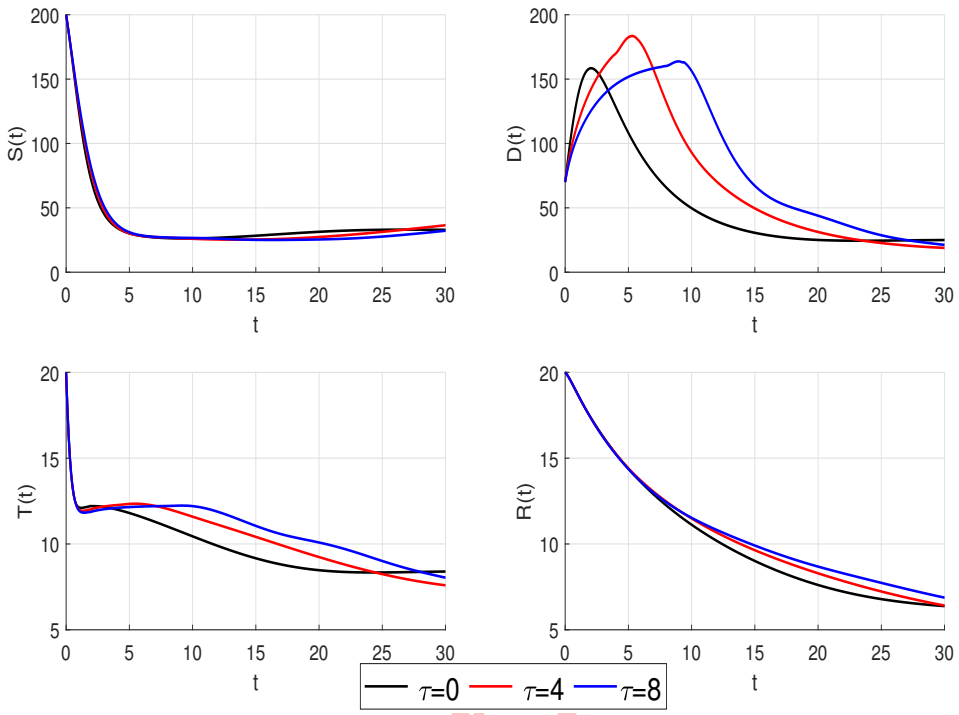

Figure 9: Parameter effect of τ on $S(t)$, $D(t)$, $T(t)$, $R(t)$

capacity.

The main lesson is that single-strategy approaches may be insufficient, because peaks and late-phase levels depend on different parameters. A combined approach is therefore needed: short-term peak management (prevention, awareness) together with late-phase addiction control (treatment access, quality, relapse prevention).

We emphasize that these conclusions are qualitative statements about parameter dependence in a stylized model. The model contains no healthcare-capacity variable, no cost functional, and no calibrated case data. Quantitative policy targets, treatment-duration structures, or cost-effectiveness conclusions would require an extension of the model along these dimensions, which we leave for future work.

Funding

This research received no specific grant from any funding agency in the public, commercial, or not-for-profit sectors.

Author contributions

S.G. and N.I.K. contributed equally to all aspects of this work. All authors have read and agreed to the published version of the manuscript.

Conflict of interest

The authors declare that they have no conflict of interest.

Code availability

The MATLAB implementation of the Taylor-wavelet collocation scheme used for all numerical results in this paper, including the residual analysis and the parametric sensitivity computations, is available from the corresponding author on reasonable request.

References

[1] K.E. Atkinson, *An Introduction to Numerical Analysis*, 2nd ed., John Wiley & Sons, New York, 1989.

[2] B. Babayar-Razlighi, *Numerical solution of an influenza model with vaccination and antiviral treatment by the Newton–Chebyshev polynomial method*, J. Math. Model. **11(1)** (2023) 103–116.

[3] A. Beler, G. Özaltun Simşek, S. Gümgüm, *Numerical solutions of the HIV infection model of CD*4^+ *cells by Laguerre wavelets*, Math. Comput. Simul. **209** (2023) 205–219.

[4] R. Bouajaji, A. Abta, H. Laarabi, M. Rachik, *Optimal control of a delayed alcoholism model with saturated treatment*, Differ. Equ. Dyn. Syst. **32** (2024) 277–292.

[5] S. Djillali, S. Bentout, T.M. Touaoula, A. Tridane, *Global dynamics of alcoholism epidemic model with distributed delays*, Math. Biosci. Eng. **18** (2021) 8245–8256.

[6] S. Gümgüm, D.E. Özdek, G. Özaltun, N. Bildik, *Legendre wavelet solution of neutral differential equations with proportional delays*, J. Appl. Math. Comput. **61** (2019) 389–404.

[7] S. Gümgüm, D.E. Özdek, G. Özaltun, *Legendre wavelet solution of high order nonlinear ordinary delay differential equations*, Turk. J. Math. **43** (2019) 1339–1352.

[8] S. Gümgüm, *Taylor wavelet solution of linear and nonlinear Lane-Emden equations*, Appl. Numer. Math. **158** (2020) 44–53.

[9] S. Gümgüm, H.M. Pişkin, *Parameter investigation of alcohol-induced liver disease using Chebyshev and Legendre polynomials*, Bull. Int. Math. Virtual Inst. **15** (2025) 357–371.

[10] S. Gümgüm, *Parametric investigation of alcohol consumption in diabetic individuals using the Gegenbauer wavelet method*, J. Mod. Technol. Eng. **10** (2025) 119–140.

[11] J. Hadadi, R. Khoshsiar Ghaziani, J. Alidousti, Z. Eskandari, *Dynamics and bifurcations of a discrete-time neural network model with a single delay*, J. Math. Model. **12(3)** (2024) 419–430.

[12] H.F. Huo, Y.L. Chen, H. Xiang, *Stability of a binge drinking model with delay*, J. Biol. Dyn. **11** (2017) 210–225.

[13] E. Keshavarz, Y. Ordokhani, M. Razzaghi, *The Taylor wavelets method for solving the initial and boundary value problems of Bratu-type equations*, Appl. Numer. Math. **128** (2018) 205–216.

[14] B. Khajji, L. Boujallal, M. Elhia, O. Balatif, M. Rachik, *A fractional-order model for drinking alcohol behaviour leading to road accidents and violence*, Math. Model. Comput. **9** (2022) 501–518.

[15] S.H. Ma, H.F. Huo, X.Y. Meng, *Modelling alcoholism as a contagious disease: a mathematical model with awareness programs and time delay*, Discrete Dyn. Nat. Soc. **2015** (2015) 260195.

[16] C.I. Nkeki, I.A. Mbarie, *On mathematical modeling and stability analysis of chickenpox models in the presence of weakened-immune individuals in a population*, J. Math. Model. (2026), in press.

[17] K.R. Prasad, M. Khuddush, K.V. Vidyasagar, *Almost periodic positive solutions for a time-delayed SIR epidemic model with saturated treatment on time scales*, J. Math. Model. **9(1)** (2021) 45–60.

[18] G. Özaltun, A. Konuralp, S. Gümgüm, *Gegenbauer wavelet solutions of fractional integro-differential equations*, J. Comput. Appl. Math. **420** (2022) 114830.

[19] G. Özaltun Simşek, A. Beler, S. Gümgüm, *Gegenbauer wavelet solutions of the SIR and the SITR systems of the COVID-19 disease*, Int. J. Biomath. (2024).

[20] G. Özaltun Simşek, S. Gümgüm, *Numerical solutions of Troesch and Duffing equations by Taylor wavelets*, Hacet. J. Math. Stat. **52** (2023) 292–302.

[21] D. Özdek, *Investigating the impact of the parameters on the model of HIV infection including a cure rate and latently infected cells*, J. Appl. Math. Comput. **71** (2025) 1831–1858.

[22] R. Thamchai, *Optimal control of a drinking epidemic model with time delay*, IAENG Int. J. Appl. Math. **55** (2025) 1205–1212.

[23] C.E. Türe, S. Gümgüm, *Modeling the impact of public and private treatment on alcohol addiction: a spectral methods approach*, Bol. Soc. Mat. Mex. **32** (2026) 19.

[24] X.Y. Wang, K. Hattaf, H.F. Huo, H. Xiang, *Stability analysis of a delayed social epidemics model with general contact rate and its optimal control*, J. Ind. Manag. Optim. **12** (2016) 1267–1285.

[25] World Health Organization, *Global Status Report on Alcohol and Health and Treatment of Substance Use Disorders*, WHO, Geneva, 2024. Available from: https://www.who.int/publications/i/item/9789240096745.

[26] H. Xiang, C.C. Zhu, H.F. Huo, *Modelling the effect of immigration on drinking behaviour*, J. Biol. Dyn. **11** (2017) 275–298.

[27] Z. Zhang, J. Zou, S. Kundu, *Bifurcation and optimal control analysis of a delayed drinking model*, Adv. Differ. Equ. **2020** (2020) 522.